AJNR

Fat-suppressed MR of the orbit and cavernous sinus: comparison of fast spin-echo and conventional spin-echo.

S K Mukherji, R P Tart, J Fitzsimmons, C Belden, S McGorray, J Guy and A A Mancuso

AJNR Am J Neuroradiol 1994, 15 (9) 1707-1714
http://www.ajnr.org/content/15/9/1707

Fat-Suppressed MR of the Orbit and Cavernous Sinus: Comparison of Fast Spin-Echo and Conventional Spin-Echo

Suresh K. Mukherji, Roger P. Tart, Jeff Fitzsimmons, Clifford Belden, Sue McGorray, John Guy, and Anthony A. Mancuso

PURPOSE: To compare T2-weighted fat-suppressed fast spin-echo imaging with fat-suppressed conventional spin-echo imaging in the detection of normal intraorbital and pericavernous anatomy and orbital disease, and to determine the efficacy of fat saturation with T2-weighted fast spin-echo imaging of the cavernous sinus. **METHODS:** Contrast-to-noise ratios of normal intraorbital anatomy were calculated and compared in 10 consecutive patients using fat-suppressed fast spin-echo and conventional spin-echo T2-weighted images. Contrast-to-noise ratios of common intraorbital lesions were calculated and compared using fat-suppressed fast spin-echo and fat-suppressed conventional spin-echo. Qualitative evaluation was performed and compared for normal intraorbital anatomy using both fat-suppressed fast spin-echo and fat-suppressed conventional spin-echo in 16 patients. Qualitative evaluation for the detection of normal anatomic structures of the pericavernous region was performed and compared using fast spin-echo with and without fat suppression and fat-suppressed conventional spin-echo T2-weighted images in 16 patients. Fat saturation was performed using standard commercially available chemical saturation technique. **RESULTS:** Reduced imaging time allowed more acquisitions for fat-suppressed fast spin-echo images, which significantly improved visibility of intraorbital and pericavernous anatomy over fat-suppressed conventional spin-echo. Anatomic visibility was also improved because of reduced motion, phase encoding, and susceptibility artifacts. There was no significant difference between contrast-to-noise ratios for fat-suppressed fast spin-echo and fat-suppressed conventional spin-echo imaging of the lateral and medial rectus muscles. Contrast-to-noise ratios of fat suppressed fast spin-echo of orbital disease was significantly greater than contrast-to-noise ratios of fat-suppressed conventional spin-echo. Detection of several normal anatomic structures of the pericavernous region was significantly improved with non–fat-suppressed fast spin-echo over fat-suppressed fast spin-echo because of significantly reduced magnetic susceptibility artifact. **CONCLUSIONS:** Fat-suppressed fast spin-echo is superior to fat-suppressed conventional spin-echo for T2-weighted orbital imaging. Non–fat-suppressed fast spin-echo is the preferred pulse sequence for T2-weighted imaging of the cavernous sinus because of the minimal susceptibility artifact.

Index terms: Orbits, magnetic resonance; Magnetic resonance, comparative studies; Magnetic resonance, fat suppression; Cavernous sinus, magnetic resonance

AJNR Am J Neuroradiol 15:1707–1714, Oct 1994

Currently, magnetic resonance (MR) and computed tomography (CT) are complementary studies for orbital imaging. Advantages of CT include detailed visualization of the bony orbit and excellent resolution between the retrobulbar fat and orbital disease. MR provides multiplanar imaging with improved soft-tissue contrast resolution in the absence of ionizing radiation. MR imaging appears to be the study of choice for evaluation of orbital disease including hemorrhagic lesions, optic neuritides,

Received June 28, 1993; accepted after revision January 19, 1994.

Supported in part by the clinical module of core grant EY-08571 from the National Eye Institute.

From the Departments of Radiology (S.K.M., R.P.T., J.F., C.B., A.A.M.), Biostatistics (S.M.), and Ophthalmology (J.G.), University of Florida College of Medicine, Gainesville.

Address reprint requests to Suresh K. Mukherji, MD, Department of Radiology, Shands Teaching Hospital, University of Florida College of Medicine, Box 100374, Gainesville, FL 32610.

AJNR 15:1707–1714, Oct 1994 0195-6108/94/1509–1707

and lesions involving the orbital apex (1). Recently, the fast spin-echo (FSE) sequence (2–5) has gained popularity as a method of acquiring T2-weighted images in a fraction of the time required for conventional spin-echo (CSE) techniques. The benefits can be used to increase the number of patients imaged in a given time or to improve the spatial resolution by increasing the matrix size, decreasing the field of view, and/or decreasing section thickness while increasing the number of acquisitions. The benefits of improved spatial resolution are especially useful in areas of detailed anatomy including the orbit and pericavernous regions.

Despite its potential benefits, FSE has not gained popularity for orbital imaging because of the high signal of the retrobulbar fat on T2-weighted sequences which could obscure subtle intraorbital disease. The increased fat signal is thought to be caused by the apparent lengthening of T2 resulting from short echo spacing inherent in FSE imaging. The contribution to the T2-decay process from lipid protons and spin-spin splittings is subsequently reduced, resulting in the apparent lengthening of T2 (2, 6, 7). The potential benefits of FSE imaging have not been achieved for orbital imaging because of this potential pitfall. The addition of fat-saturation techniques to FSE imaging could provide the benefits associated with FSE imaging of the orbits without sacrificing lesion detectability.

The purpose of this study is to evaluate the detectability of normal orbital anatomy and orbital disease with fat-suppressed FSE and compare it with fat-suppressed T2-weighted CSE. In addition, we evaluated FSE with and without fat-suppression and CSE with fat suppression for imaging the pericavernous region in order to determine the optimal T2-weighted sequence for imaging this area.

Subjects and Methods

We quantitatively evaluated fat-suppressed CSE and fat-suppressed FSE for the detection of normal intraorbital anatomy in the following manner. Ten consecutive patients with clinical suspicion of orbital disease underwent fat-suppressed FSE and fat-suppressed CSE T2-weighted coronal MR imaging of the orbits. The signal intensities (SI) of both the medial and lateral rectus muscles, orbital fat, and background were obtained by the placement of regions of interests in the coronal plane. Signal-to-noise ratio was calculated as SI(area)/SD(background). Contrast-to-noise ratios were calculated using the following formula: [SNR(muscle) − SNR(fat)]/SD(bkg). Paired t test was used to test for significant differences between results from the different pulse sequences.

Quantitative comparison for orbital lesions was performed in the following manner. Ten patients with known orbital disease underwent fat-suppressed FSE and fat-suppressed CSE. These 10 patients had the following 11 lesions.

Lesion	Number
Optic neuritis	2
Meningioma	3
Hemangioma	3
Optic glioma	2
Wegener granulomatosis	1
Total	**11**

Signal intensities of the lesion, orbital fat, and background were obtained by placing regions of interest through the respective areas. Signal intensities were obtained in those patients with optic neuritis by placing regions of interest in the coronal plane of the affected optic nerve. Signal-to-noise and contrast-to-noise of the lesions were calculated with the same formulas for both fat-suppressed FSE and fat-suppressed CSE. Paired t test was used to test for significant differences between results from the different pulse sequences.

Diagnosis of optic gliomas and Wegener granulomatosis was based on previous biopsy. Diagnosis of optic neuritis was based on a history of multiple sclerosis with recent onset of unilateral reduction in visual acuity in combination with characteristic clinical findings. Diagnoses of meningioma and hemangioma were based on clinical findings of reduced vision in combination with the characteristic radiographic appearance.

Qualitative evaluation of the orbits was performed in the following manner. Sixteen consecutive patients clinically suspected of having intraorbital disease underwent coronal fat-suppressed FSE and fat-suppressed CSE T2-weighted imaging. Assessment of visibility of normal intraorbital anatomic structures was performed by two neuroradiologists with the final result reached by consensus. Grading was based on a 1-to-5 scale: 1 indicates nonvisualization; 3, indeterminate; and 5, definite visualization. Intraorbital anatomic structures evaluated included extraocular muscles, superior ophthalmic vein, and the supraorbital nerve/vein complex. The evaluation of the optic nerve sheath complex was graded on a 1-to-5 scale: 1 indicates inability to identify complex; 3, identification of complex without separation of optic nerve from optic sheath; and 5, distinct separation of optic nerve from sheath. Although a 1-to-3 scale may have been used, we preferred a 1-to-5 scale to reflect better the varying degrees of uncertainty that may arise from a subjective grading system. Artifacts attributed to magnetic susceptibility from the paranasal sinuses, motion, and phase encode were also graded on a separate 1-to-5 scale: 1 indicates obscuration of surrounding anatomic structures caused by artifact; 3, artifact present but structures distinguishable;

and 5, no artifact present. For bilateral anatomic structures, an average score was calculated. Regions altered by disease or prior surgical intervention were not evaluated; only the value of the normal side was used. A single value was used to evaluate artifacts.

Analysis of these ordinal data was performed as follows. For each person and anatomic structure, the difference between fat-suppressed FSE and fat-suppressed CSE gradings was calculated. Wilcoxon signed rank tests were performed on these differences for each anatomic region to test whether the median difference is zero (ie, no difference between FSE and CSE grades). A *P* value of .05 or less is considered statistically significant.

Analysis of the pericavernous region was performed in the following manner. The same 16 patients as above underwent coronal fat-suppressed FSE and fat-suppressed CSE T2-weighted imaging from the anterior pons to the superior orbital fissure. Sixteen additional patients underwent coronal non–fat-suppressed FSE of the same region. Assessment of the visualization of normal pericavernous structures was performed by two neuroradiologists with the final result reached by consensus. Grading was based on a 1-to-5 scale: 1 indicates nonvisualization; 3, indeterminate; and 5, definite visualization. Pericavernous anatomic structures analyzed included the dural reflection of the cavernous sinus, adjacent cranial nerves (II, III, IV, gasserian ganglion, V1, V2, V3), pituitary gland, pituitary stalk, and flow voids within the carotid arteries. Magnetic susceptibility artifact from the sphenoid sinus, phase-encode artifact from the carotid arteries, and motion artifact attributable to patient motion was graded on a 1-to-5 scale: 1 indicates obscuration of surrounding anatomic structures caused by artifact; 3, artifact present but able to distinguish structures; and 5, no artifact present.

Because the fat-suppressed FSE and fat-suppressed CSE sequences were performed on the same patients, Wilcoxon signed rank tests were again used to test for differences in grades of the pericavernous region. Because the fat-suppressed and non–fat-suppressed evaluations were performed on different groups of patients, Wilcoxon rank sum tests were used to assess whether the median grades differed for fat-suppressed and non–fat-suppressed FSE evaluation for each region scored. A *P* value of .05 or less is considered statistically significant.

All MR examinations were performed on a 1.5-T General Electric Signa (Milwaukee, Wis) using a standard quadrature head coil. FSE MR parameters used in imaging the orbit and pericavernous region were 4000–6000/95/4 (repetition time/echo time/excitations) with a 16 pulse echo train. Repetition time was varied based on the amount of volume imaged in each individual examination. Matrix size was 256 × 192 or 256 × 256 with a section thickness of 3- to 4-mm with a 0.5-mm interspace gap. All studies were performed with a 16 field of view. Maximum imaging time with fat-suppressed FSE using a 256 × 256 matrix and 4 excitations was 6 minutes and 24 seconds. CSE parameters were 2000/90/1 performed with a 256 × 192 matrix and 16 field of view with a total imaging time of 7 minutes and 29 seconds. The imaging parameters for FSE and CSE were intentionally different because our aim was to optimize these imaging sequences for clinical use, rather than keep the parameters constant for a purely experimental comparison. Fat suppression was performed using standard frequency selective saturation technique, currently available on Signa units.

TABLE 1: Comparison of conventional and fast spin-echo fat-suppressed images for evaluation of the orbital region in 16 patients

Site	Median Value, [FSE − CSE]	*P* Value
Optic nerve–optic sheath complex	0.88	.0002[a]
Superior opthalmic vein	0.5	.0002[a]
Extraocular muscles		
Medial rectus	0	1
Lateral rectus	0	.34
Superior rectus	0	.75
Inferior rectus	0	.75
Superior oblique	0	.75
Levator palpebra	0.25	.07
Supraorbital nerve-vein complex	0.5	.19
Susceptibility	1.25	.35
Motion	0	.91

[a] $P < .05$, Wilcoxon signed rank test.

Results

Orbital Region

Results are summarized in Table 1. Overall image quality of fat-suppressed FSE was superior to fat-suppressed CSE. Quantitative evaluation of normal intraorbital anatomy demonstrated no significant difference between contrast-to-noise ratio of fat-suppressed FSE and that of fat-suppressed CSE of the medial and lateral rectus muscles. However, contrast-to-noise ratio of fat-suppressed FSE of orbital lesions was significantly greater ($P < .0006$) than that of fat-suppressed CSE (Figs 1 and 2).

Qualitative evaluation demonstrated significantly increased visibility of the optic nerve and superior ophthalmic vein with fat-suppressed FSE imaging. The supraorbital nerve-vein complex and the levator palpebrae muscle tended to be better seen on the fat-suppressed FSE sequences. There was no significant difference between the two sequences for the presence of phase-encode, motion, or magnetic susceptibility artifacts involving the orbital region.

FSE allowed consistent separation of the optic nerve from the surrounding cerebrospinal fluid within the optic sheath. Measurements of the diameter of the optic nerve and the optic sheath were performed at a location 1 cm pos-

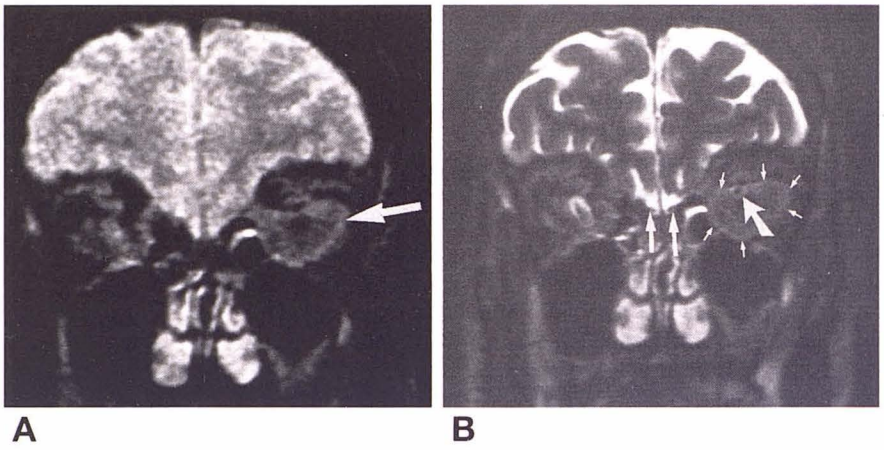

Fig 1. Optic nerve sheath meningioma: coronal T2-weighted images.

A, Fat-suppressed CSE images demonstrate a left intraorbital mass (*arrow*) inseparable from the left optic nerve.

B, Fat-suppressed FSE images demonstrate partial encasement of the left optic nerve sheath (*slanted arrow*) by the mass (*small arrows*), thus suggesting the diagnosis of a meningioma. Note improved visibility of the olfactory nerves (*large arrow*).

terior to the nerve-globe junction in all 16 patients. The average diameters of the optic nerve and optic sheath at this level were 2.8 mm and 5.8 mm, respectively.

Pericavernous Region

Overall image quality of fat-suppressed FSE was superior to that of fat-suppressed CSE: many anatomic structures in the pericavernous region were better seen with fat-suppressed FSE (Table 2). The dural reflection, cranial nerve II, cranial nerve III, gasserian ganglion, V2, V3, pituitary gland, and the infundibulum were significantly increased with the fat-suppressed FSE sequence. Visualization of the pericavernous region was improved on fat-suppressed FSE because of the significant reduction in magnetic susceptibility and phase-encode artifacts.

Non–fat-suppressed FSE significantly improved the visibility of several pericavernous structures including the dural reflection, cranial nerve III, gasserian ganglion, V1, V2, and V3 over fat-suppressed FSE imaging (Table 3). Non–fat-suppressed FSE significantly reduced magnetic susceptibility artifact arising from the skull base and sphenoid sinus.

Discussion

CSE imaging has been the standard pulse sequence for neuroophthalmologic imaging since the introduction of MR to diagnostic imaging. The addition of fat suppression has improved the detectability of intraorbital lesions on T1-weighted imaging (8). Because the imaging time is long, T2-weighted CSE images are often degraded by patient motion thereby limiting the diagnostic ability of this sequence. To minimize the lengthy acquisition time, CSE T2-weighted imaging is often limited to one acquisition with a reduced matrix size thereby reducing signal-to-noise ratio and spatial resolution. Larger fields

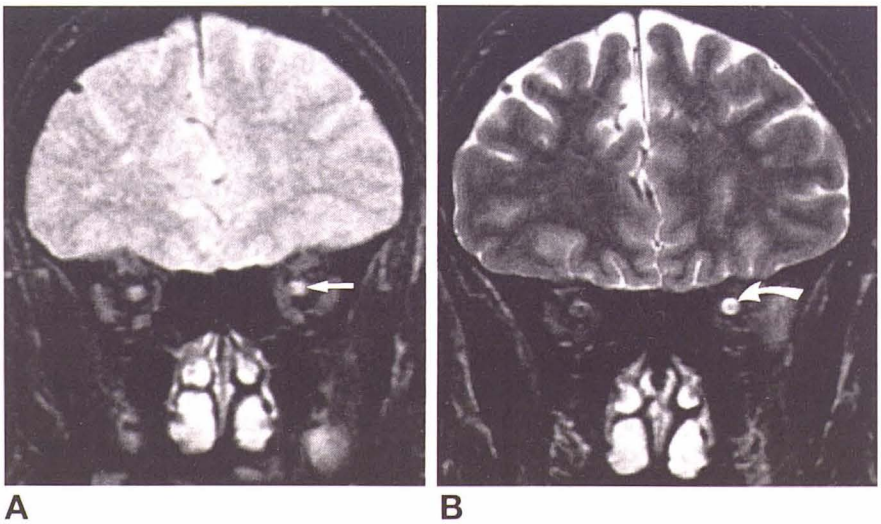

Fig 2. Coronal T2-weighted images of left optic neuritis.

A, Fat-suppressed CSE demonstrates mildly increased signal within the left optic nerve-sheath complex.

B, Fat-suppressed FSE images show unequivocal increased signal within both the optic nerve and optic sheath (*curved arrow*).

TABLE 2: Comparison of conventional spin-echo (CSE) and fast spin-echo (FSE) fat-suppressed images for evaluation of the pericavernous region in 16 patients

Site	Median Value [FSE − CSE]	*P* Value
Dural reflect	0.75	.0001[a]
Cranial nerve II	1.25	.0048[a]
Cranial nerve III	0.88	.0055[a]
Cranial nerve V		
Ganglion	0.88	.0132[a]
V1	0.5	.0781
V2	0.75	.0001[a]
V3	0.5	.0251[a]
Flow voids in internal carotid artery	0.38	.0039[a]
Pituitary gland	1	.0073[a]
Infundibulum	2	.0012[a]
Susceptibility artifact	1.25	.0005[a]
Motion artifact	0	.3125
Phase-encode artifact	2	.001[a]

[a] $P < .05$, Wilcoxon signed rank test.

of view are necessary to obtain adequate contrast resolution. The overall effect is a sequence with suboptimal image quality that limits the diagnostic capability of the study.

Because of reduced imaging time, FSE offers many advantages over CSE T2-weighted imaging. Spatial resolution can be increased by acquiring a larger matrix size while still maintaining a relatively short imaging time. Increased signal-to-noise ratios and contrast resolution can be improved by increasing the number of acquisitions without prolonging imaging time. Increased contrast resolution allows a reduction in the field of view, which improves visualization of smaller anatomic structures. Alternatively, because FSE can reduce acquisition time to less than one fourth that of CSE, the number of patients imaged over time may be significantly increased if identical imaging parameters are used (1).

In this study, a portion of the time savings was sacrificed in order to improve image quality by increasing the number of acquisitions (n = 4), which increased the contrast resolution and allowed a reduced field of view. Spatial resolution was improved by increasing the matrix size by incorporating more phase-encode steps (192 or 256). Despite these changes, acquisition times for orbital and pericavernous imaging were still 1 to 2 minutes less than fat-suppressed CSE imaging.

For orbital imaging, overall image quality of fat-suppressed FSE was superior to fat-suppressed CSE. There was no quantitatively or qualitatively significant difference in visualization of normal intraorbital anatomic structures. In fact, small detailed anatomic structures such as the levator palpebrae muscle and superior ophthalmic nerve-vein complex tended to be better seen on the fat-suppressed FSE sequences (Fig 3). Visualization of the latter structure is especially important because it is a common path of perineural spread for tumors that arise in the periorbital region. Asymmetric enlargement of this complex in the presence of an adjacent tumor may alter patient treatment.

Quantitatively, intraorbital lesion conspicuity was significantly greater with fat-suppressed

TABLE 3: Comparison of fat-suppressed and non–fat-suppressed fast spin-echo imaging for evaluation of the pericavernous region in 16 patients

Site	Fat-suppressed		Non–fat-suppressed		*P* Value
	Mean Value	Median Value	Mean Value	Median Value	
Dural reflect	4.3	4	4.75	5	.0110[a]
Cranial nerve II	4.64	5	5	5	.058
Cranial nerve III	3.69	4	4.48	4.5	.0129[a]
Cranial nerve V					
Ganglion	4	4	5	5	.0001[a]
V1	2.82	3	3.8	3.5	.0005[a]
V2	3.46	3.5	4.31	4.5	.0014[a]
V3	3.38	3.5	4.18	4.5	.0131[a]
Flow voids in internal carotid artery	4.82	5	4.94	5	.6064
Pituitary gland	4.59	5	4.95	5	.1669
Infundibulum	4.46	5	4.85	5	.5893
Susceptibility artifact	3.69	4	4.81	5	.0001[a]
Motion artifact	4.97	5	5	5	.4595
Phase-encode artifact	4.75	5	4.88	5	.1811

[a] $P < .05$, Wilcoxon's Rank Sum Test.

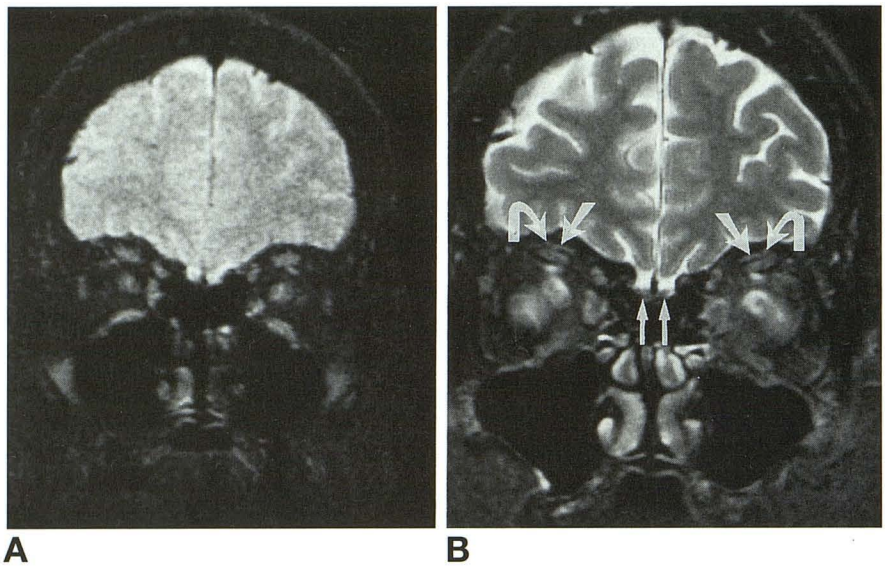

Fig 3. Coronal T2-weighted images of the orbit.

A, Fat-suppressed CSE through orbits demonstrates adequate visibility of the normal intraorbital structures.

B, Fat-suppressed FSE image demonstrates improved visibility over the fat-suppressed CSE image (*A*) of the supraorbital nerve-vein complex (*curved arrows*), levator palpebrae muscle (*slanted arrows*), and olfactory complex (*straight arrows*).

FSE than with fat-suppressed CSE, because signal-to-noise ratios of the lesion increased as a result of the increased number of acquisitions used for the fat-suppressed FSE sequence. Patients with optic neuritis had higher signal intensity within the optic nerve and surrounding cerebrospinal fluid on the involved side than the uninvolved side (Fig 2). An improperly placed region of interest that inadvertently includes the surrounding cerebrospinal fluid may increase by artifacts the signal-to-noise and contrast-to-noise ratios of the optic nerve. Extreme care should be taken for proper placement of the regions of interest to prevent false readings if this technique is used for optic nerve signal measurements.

In this study, we used a frequency-selective saturation technique which provided ample reduction in the signal from retrobulbar fat. Chemical shift artifact which could occur at fat-water interfaces (8) was not present on the fat-suppressed FSE images. Inversion recovery fat nulling (short-inversion-time inversion recovery [STIR]) is an alternative technique for orbital imaging that would likely yield contrast-to-noise ratios results similar to ours. However, STIR FSE appears more prone to motion and flow-related artifact which reduce image quality (9).

FSE was superior to CSE for fat-suppressed imaging of the pericavernous region. Overall image quality was improved with fat-suppressed FSE as a result of modifications in image acquisition techniques discussed above. In addition, image quality was also improved because of a significant reduction in susceptibility and phase-encode artifacts, which were present on the fat-suppressed CSE images. Phase-encode artifacts arising from carotid pulsations, which limited visualization on the fat-suppressed CSE sequences, were significantly reduced on the fat-suppressed FSE sequences (Fig 4). The reduction is likely attributable to a decrease in misregistration as a result of the frequent radio frequency pulses in the echo train of the FSE sequence.

Susceptibility artifact from the aerated sphenoid sinus and skull base also inhibited anatomic visualization with fat-suppressed CSE imaging. This was also reduced with fat-suppressed FSE. Interestingly, the use of non–fat-suppressed FSE T2-weighted imaging further improved image quality by providing images almost completely free of all susceptibility artifact (Fig 4). Decreased sensitivity of FSE imaging to susceptibility artifact has been described in previous reports (1, 7, 10, 11). The decreased sensitivity is felt to result from a reduction in diffusion losses caused by the frequent radio frequency pulses that compose the echo train. In our study, the use of a frequency-selective saturation fat-suppression technique slightly increased the magnetic susceptibility artifact, which degraded visualization of this region. Because it does not use a frequency-selective pulse, STIR imaging may provide fat suppression devoid of susceptibility artifact when used in conjunction with FSE for imaging this region.

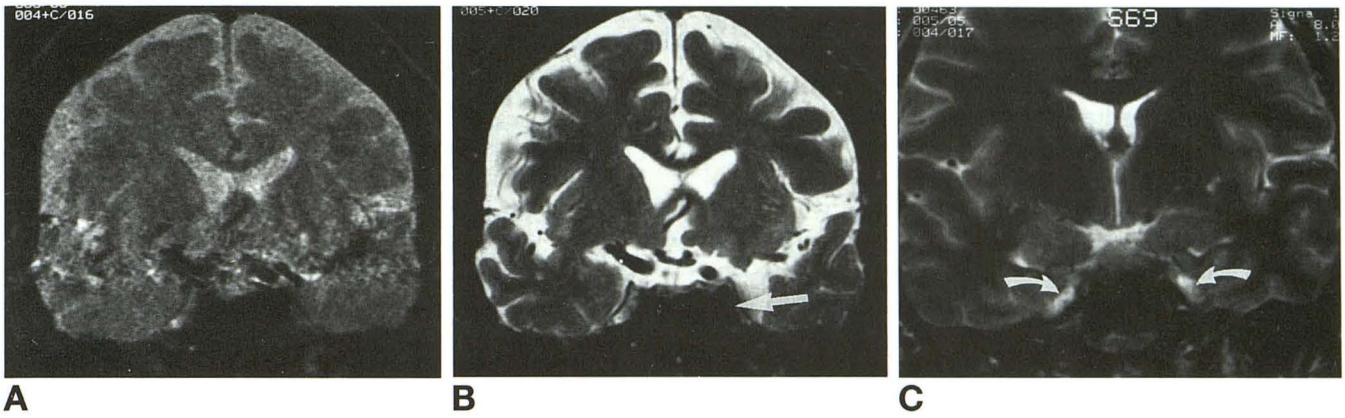

Fig 4. Coronal T2-weighted imaging of the cavernous sinus at the level of the fifth nerve ganglion.

A, Fat-suppressed CSE demonstrates image degradation caused by phase-encode and magnetic susceptibility artifacts.

B, Fat-suppressed FSE of same patient shows improved image quality with complete resolution of phase-encode artifact. Although magnetic susceptibility artifact is significantly reduced, residual artifact obscures visualization of the left fifth nerve ganglion (*arrow*).

C, Non–fat-suppressed FSE in a different patient allows visualization of the component nerve rootlets within both ganglion (*curved arrows*) because of a lack of susceptibility artifact.

The reduction in susceptibility artifact in the non–fat-suppressed FSE images resulted in sharper delineation of bone–soft tissue interfaces than in the fat-suppressed FSE images. This resulted in further improvements in identification of the detailed anatomy of this region (Fig 5). In this study, significant reductions in susceptibility artifacts correlated with significant improvements in visualization of the dural reflection and several cranial nerves within the cavernous sinus. Recent studies have determined that preoperative imaging studies may help predict the difficulty of resecting cavernous sinus meningiomas and the likelihood of certain postoperative complications (12). The improved anatomic visualization with non–fat-suppressed FSE may be helpful for appropriate preoperative planning and assessment of potential surgical complications.

In conclusion, FSE provides rapid T2-weighted imaging of the orbits and pericavernous region. Fat-suppressed FSE provides superior image quality and improved lesion conspicuity over fat-suppressed CSE, and is the preferred T2-weighted sequence for evaluation of the orbit. Non–fat-suppressed FSE was the pre-

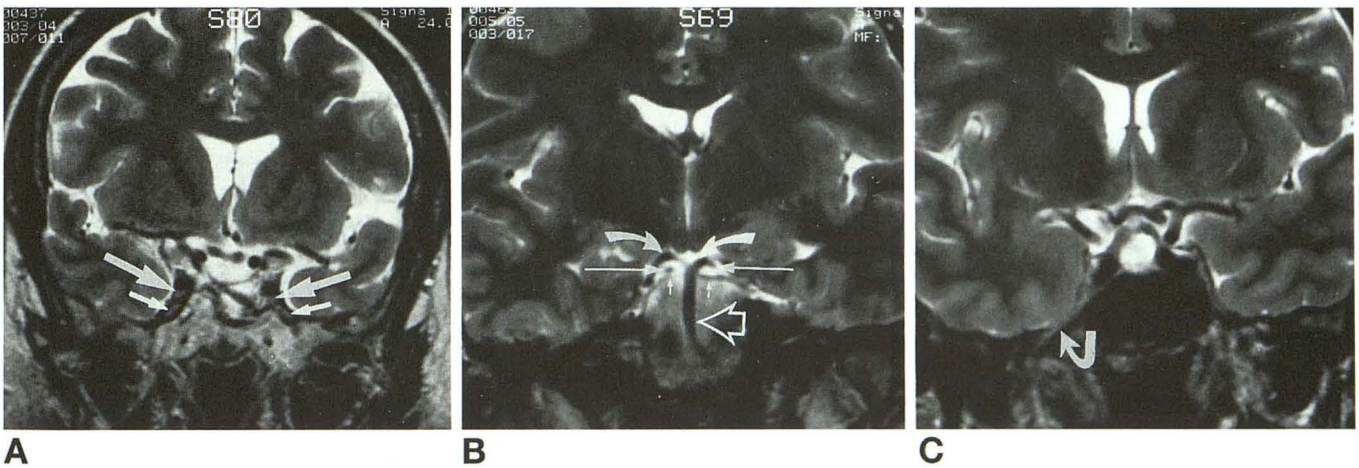

Fig 5. Non–fat-suppressed FSE imaging of normal anatomic structures of the pericavernous region.

A, V1 (*large arrows*) and V2 (*small arrows*).

B, Cranial nerve III (*long arrows*) as it crosses inferior to the posterior cerebral artery (*curved arrows*) and above the superior cerebellar artery (*small arrows*). Note excellent visibility of basilar artery (*open arrow*) and of the origin of the left superior cerebellar artery from the basilar artery.

C, V3 (*curved arrow*) as it courses through foramen ovale into the masticator space.

ferred technique for T2-weighted imaging of the pericavernous region because of its minimal magnetic susceptibility artifact which improved visualization of adjacent structures.

References

1. Atlas SW. *Magnetic Imaging of the Brain and Spine.* New York: Raven Press, 1991:710–712
2. Ahn SS, Mantello MT, Jones KM, et al. Rapid MR imaging of the pediatric brain using fast spin-echo technique. *AJNR Am J Neuroradiol* 1992;13:1169–1177
3. Henning J, Naureth A, Friedberg H. RARE imaging: a fast imaging method for clinical MR. *Magn Reson Med* 1986;3:823–833
4. Henning J, Friedberg H. Clinical applications and methodological developments of the RARE technique. *Magn Reson Imaging* 1988; 6:391–395
5. Mulkern RV, Wong STS, Winalski C, Jolesz FA. Contrast manipulation and artifact assessment of 2D and 3D RARE sequences. *Magn Reson Imaging* 1990;8:557–566
6. Melki PS, Mulkern RV, Panych LP, Jolesz FA. Comparing the FAISE method with conventional dual echo sequences. *Magn Reson Imaging* 1991;1:319–326
7. Allerhand A. Analysis of Carr-Purcell spin-echo NMR experiments on multiple-spin systems, 1: the effect of homonuclear coupling. *J Chem Phys* 1966;44:1–9
8. Lee DH, Simon JH, Szumowski J, et al. Optic neuritis and orbital lesions: lipid suppressed chemical shift MR imaging. *Radiology* 1991;179:543–546
9. Jones KM, Mulkern RV, Schwartz RB, Oshio K, Barnes PD, Jolesz FA. Fast spin echo imaging of the brain and spine: current concepts. *AJR Am J Roentgenol* 1992;158:1313–1320
10. Bendel P. Spin-echo attenuation by diffusion in non-uniform field gradients. *J Magn Reson* 1990;86:509–515
11. Norbash AM, Glover GH, Enzman DE. Intracerebral lesion contrast with spin-echo and fast spin echo pulse sequences. *Radiology* 1992;185:661–665
12. Hirsch WL, Sekhar LN, Lanzino G, Pomonis S, Sen CN. Meningiomas involving the cavernous sinus: value of imaging for predicting surgical complications. *AJR Am J Roentgenol* 1993;160: 1083–1088